# Highly Porous Pillared Clay with Multistacked $SiO_2/TiO_2$ Nanosols

**Jin-Ho Choy*, Joo-Hyoung Park, and Joo-Byoung Yoon**

*Department of Chemistry, Center for Molecular Catalysis, College of Natural Sciences, Seoul National University, Seoul 151-742, Korea*

*Received June 2, 1998*

Layered nanocomposite, $SiO_2/TiO_2$ sol pillared clay, has been prepared by the ion exchange reaction of $Na^+$ ion in montmorillonite with positively charged mixed $SiO_2/TiO_2$ sol. The nanosized sol particles were synthesized by mixing $SiO_2$ sol solution with $TiO_2$ one, which is obtained by acidic hydrolysis of TEOS and $TiCl_4$, respectively. From powder XRD, the basal spacing ($d_{001}$) of the sample calcined at 400 °C was found to be *ca.* 60 Å, due to the multistacking of nanosized $SiO_2$ and $TiO_2$ sol particles, which was confirmed by the pore size analysis from $^{129}Xe$ NMR and micropore analysis calculated from nitrogen adsorption. The BET specific surface area shows the value of 684 $m^2g^{-1}$ (Langmuir 1115 $m^2g^{-1}$), which is the highest among various pillared clays ever reported previously, and the total porosity is found to be 0.51 $mlg^{-1}$, and the pores are mainly composed of micropore with a size of *ca.* 11.8 Å. This result agrees with the adsorption capacity obtained from water adsorption. According to diffuse reflectance ultraviolet-visible spectroscopy, it is found that the $TiO_2$ particles stabilized in the interlayer space of montmorillonite are quantum-sized of *ca.* 20 Å.

## Introduction

It is well known that smectite clays are composed of stacked two dimensional aluminosilicate layers, and are able to accommodate with a variety of ions, metal clusters, and organic molecules in the interlayer space as a result of their swelling capability caused by the suitable layer charge (< 0.6/ half unit cell). In order to obtain a new family of intercalation-type nanocomposites with high surface area and good thermal stability, various voluminous hydroxymetal cations such as $[Al_{13}O_4(OH)_{24}]^{7+}$, $[Zr_4(OH)_{14}]^{2+}$, $[Cr_n(OH)_m]^{3n-m}$, $[Fe_3O(OCOCH_3)_6]^+$, etc., have been intercalated into the smectite layers, and transformed into the inorganic oxides such as $Al_2O_3$, $ZrO_2$, $Cr_2O_3$, $Fe_2O_3$, etc. by thermal treatment to keep the interlayer space more open and rigid.[1-4] The mixed oxide sol particles such as $SiO_2$-$TiO_2$, $SiO_2$-$Fe_2O_3$, and $SiO_2$-$ZrO_2$, etc.,[5-8] have been also used as pillaring agents to enhance the thermal stability, resulting in the formation of a large basal spacing of about 20Å-50 Å which gives rise to the high porous structure with micro- or mesopores. Such porous materials were stable up to 500 °C and their specific surface areas were estimated as large as about 300-500 $m^2g^{-1}$. Therefore the pillaring reaction could be one of the most powerful route in exploring new types of porous nanocomposites with mixed sol particles. Such pillared smectites are expected to be very useful as catalyst, molecular sieve, selective adsorbent, membrane, sensor, etc.[9-11]

The $SiO_2$-$TiO_2$ pillared clay[6-8] is especially interesting because the possibility to obtain the small sized semiconductor particles below 5 nm stabilized in the interlayer space of montmorillonite, having higher photocatalytic activities than bulk ones. Since the pore size, internal surface area, and thermal stability of the pillared clays are strongly dependent upon the nature of pillaring agents and pillaring condition, it is necessary to set up new strategies to design tailor-making pillared materials by controlling the pillaring parameters.

In the present study, our research objective is to synthesize the nanocomposite with fourfold multistacked $SiO_2$ and $TiO_2$ sol particles between the layers of montmorillonite by taking advantage of the aggregation of nanosized $SiO_2$ sols and nanosized $TiO_2$ ones obtained by highly acidic hydrolysis of TEOS and $TiCl_4$, respectively, and to characterize the interlayer structure of the nanocomposite using powder X-ray diffraction (XRD), nitrogen adsorption-desorption isotherm, and diffuse reflectance ultraviolet-visible (UV/Vis) and $^{129}Xe$ nuclear magnetic resonance ($^{129}Xe$ NMR) spectroscopies.

## Experimentals

The montmorillonite clay (Kunimine-F) was used as the starting host material, and its structural formula was determined to be $Na_{0.35}K_{0.01}Ca_{0.02}(Si_{3.89}Al_{0.11})(Al_{1.60}Mg_{0.32}Fe_{0.08})O_{10}(OH)_2 \cdot nH_2O$ with a layer charge density of $0.31e^-/(Si,Al)_4O_{10}$ which was estimated by n-alkylammonium method.[12] The $Na^+$-activated one was prepared by treating the colloidal clay fractions with 1 N sodium chloride solution, and then it was washed thoroughly with doubly distilled water. An 1 wt% aqueous suspension of montmorillonite was pre-swelled for one day before using for ion exchange reaction.

A silica sol solution was prepared by mixing $Si(OC_2H_5)_4$, 2 N HCl, and ethanol with a ratio of 13.6 mL/3.5 mL/3.0 mL at room temperature. Titanium tetrachloride, $TiCl_4$, was also hydrolyzed by adding it into 1 N HCl solution with a molar ratio of $HCl/TiCl_4$=6. Each silica and titania sol solution was intermixed with a molar ratio of Si/Ti=10/1 and the mixture was stirred for 1 hour at room temperature.

The ion exchange reaction was carried out by titrating the mixed solution into the clay suspension with a ratio of Si/Ti/clay=20 mmol/2 mmol/1 g. The mixture was allowed to stand for 40 h at 75 °C, to exchange the $Na^+$ ions with the mixed $SiO_2$ and $TiO_2$ sol particles completely. Each reaction product was separated by centrifugation, washed thoroughly

*To whom all correspondence should be addressed.

with deionized water (QMST-wet), and dried in an oven at 80 °C for 24 h (QMST-80). Finally the dried sample was calcined at 400 °C for 2 h to produce the intercalation-type nanocomposite, hereafter will be abbreviated as QMST-400.

Powder XRD patterns for the orientated samples were recorded using a Philips PW1830 diffractometer with Ni-filtered Cu-K$\alpha$ radiation ($\lambda$=1.54184 Å).

Thermogravimetry-differential thermal analyses (TG-DTA) were performed on a Rigaku TAS-100 with a heating rate of 10 °C $min^{-1}$ under an ambient atmosphere.

Chemical analyses for the samples, fused with lithium metaborate at 900 °C and then dissolved in a 3% $HNO_3$ solution, were carried out with the inductively coupled plasma (ICP: Shimazu ICPS-5000) method.

UV/Vis spectra were recorded on a Perkin-Elmer Lambda 12 spectrometer equipped with an integrating sphere of 60 mm in diameter using $BaSO_4$ as a standard.

$^{129}Xe$ NMR spectroscopic analyses were performed using a Bruker AMX-400 Fourier-transform NMR spectrometer with a frequency of 110.7 MHz at 25 °C, typically under conditions with a 6 second pulse and a pulse delay of 2 second. The reference signal of xenon was taken as the signal of 304 kPa of xenon gas, which was extrapolated to zero pressure, using Jameson equation.[13] The samples were dried at 300 °C in a vacuum, and sealed at very low pressure (20 torr) of xenon gas.

Nitrogen adsorption-desorption isotherm was measured volumetrically at the liquid nitrogen temperature with a home-made computer-controlled measurement system. The calcined sample was degassed at 300 °C for 2 h, under vacuum prior to test.

Water adsorption-desorption isotherm was measured gravimetrically at 25 °C by using a CAHN-1000 balance. About 50 mg of the sample was degassed at 300 °C for 2 h, under vacuum prior to test.

## Results and Discussion

**Pillaring reaction of small sized $SiO_2$ and $TiO_2$ sol particles in the interlayer space of montmorillonite.** According to powder XRD, the basal spacings of QMST-80 and QMST-400 were determined to be 63.0 Å and 60.0 Å, respectively. It is noticeable that their interlayer distances estimated by subtracting the thickness of aluminosilicate layer (9.6 Å) from the basal spacing show supergallery heights in the range of 50.4 Å-53.4 Å. Though the basal spacing decreases gradually upon heating, the lamella structure seems to be maintained at least up to 500 °C, which is well consistent with the results of thermal analysis.

$Na^+$-montmorillonite and QMST-400 have been quantitatively analyzed by ICP to estimate the pillar contents of $SiO_2$, and $TiO_2$. Assuming that the chemical composition of aluminosilicate layer is unchanged during the pillaring reaction, the chemical composition of the pillared product can be determined as $[Si_{5.84}O_{11.68}Ti_{3.23}O_{6.46}](Si_{3.89}Al_{0.11})$ $(Al_{1.60}Mg_{0.32}Fe_{0.08})O_{10}(OH)_2$. From the calculated result, the amount of intercalated $SiO_2$ and $TiO_2$ sols is larger than that of aluminosilicate layer, and the Ti/Si molar ratio of interlayer sols is higher than that of mixed sol solution used, indicating that the intercalated layer is thicker than the host aluminosilicate layer (supergallery), and that the $TiO_2$ sol particles have stronger affinity to the negative silicate layers than the $SiO_2$ ones, which is in consistent with the fact that the $TiO_2$ sol is more positively charged than the $SiO_2$ one in this synthetic condition.

**Pore characterization.** Figure 1(a) shows the nitrogen adsorption-desorption isotherm of QMST-400. The isotherm, characterized by the Type IV according to the BDDT (Brunauer, Deming, Deming, and Teller) classification, exhibits relatively large hysteresis, whose loop is of the Type B in Boers five types,[14,15] indicating the presence of the open slit-shaped capillaries with very wide bodies and narrow short necks. It gives a good fit on the Langmuir equation as well as the BET one with a limited number of adsorption points below 0.4 relative pressure (P/Po), suggesting that it contains both micro and mesopores. It is noteworthy here that this new pillared clay could be reproducibly prepared with a remarkably high BET surface area of 684 $m^2g^{-1}$ (Langmuir=1115 $m^2g^{-1}$) and a porosity of 0.51 $mlg^{-1}$, respectively, which are highest values so far reported.

Micropore of QMST-400 was analyzed by MP method[15] as shown in Figure 1(b). Here, slit width is twice the statistical thickness (t) obtained from the standard t-curve (Harkins-Jura equation).[15] According to the MP method, the total porosity was found to be mainly composed of the micropore (0.37 $mlg^{-1}$) with a average pore size of *ca.* 11.8 Å though its gallery height was in the size of mesopore, indicating that QMST-400 is the nanocomposite with multistacked $SiO_2/TiO_2$ sol particles between the layers of montmorillonite.

The water adsorption-desorption isotherm was measured for QMST-400 as shown in Figure 2. The adsorbed amount of water increases linearly with the relative vapor pressure, and the desorption branch does not meet the adsorption one, even at a very low relative pressure, indicating also an irreversible adsorption-desorption behavior on the surface of pillars and host lattices by means of chemical reaction such as hydroxylation and hydration. The water adsorption fits more on the BET equation than on the Langmuir one,

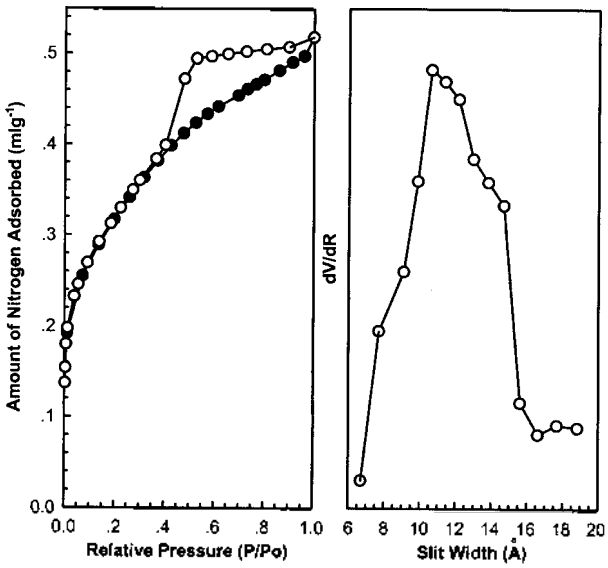


**Figure 1.** (a) Nitrogen adsorption-desorption isotherm and (b) micropore analysis for QMST-400.

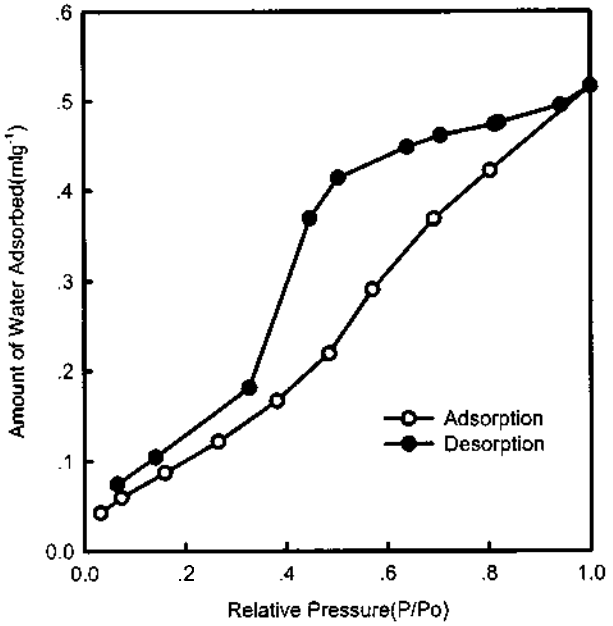


**Figure 2.** Water adsorption-desorption isotherm for QMST-400.

suggesting that the most of pores in the sample could be filled by multilayer adsorption of water molecules.

In order to investigate the microporous structure of QMST-400 in detail, $^{129}$Xe NMR spectroscopic study has been performed. $^{129}$Xe NMR spectra of xenon adsorbed in QMST-400 are shown in Figure 3(a) together with that of 304 kPa xenon gas as a reference for comparison. The chemical shift of xenon adsorbed in a cavity corresponds to the following equation[13,16]

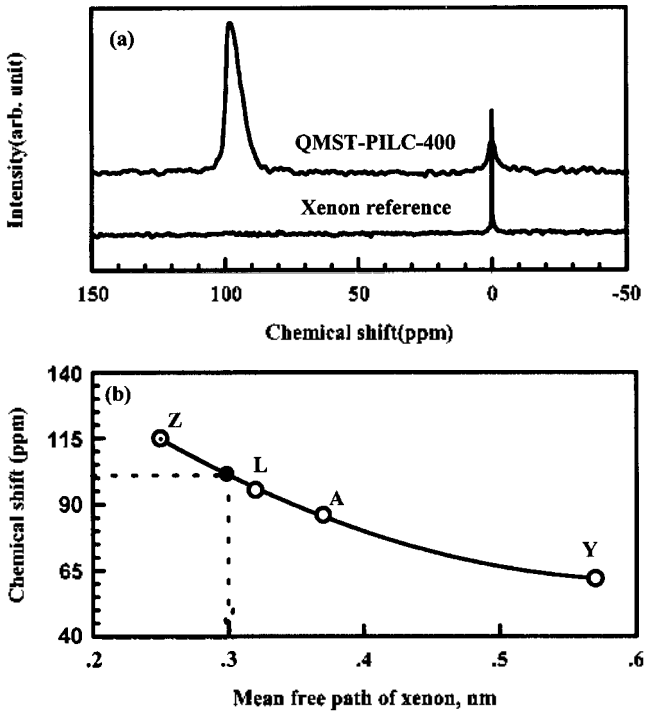


**Figure 3.** (a) $^{129}$Xe NMR spectra for QMST-400, and Xe reference. (b) Relationship between chemical shift and the mean free path of xenon adsorbed in the cavity of zeolite Z, L, A, and Y.

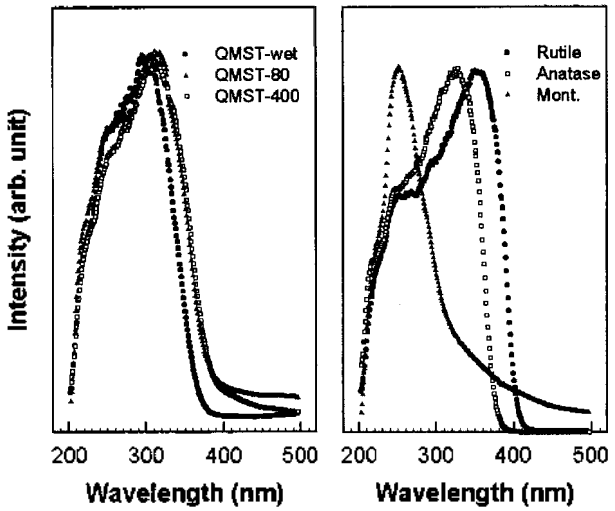


**Figure 4.** Ultraviolet-visible spectra for (a) QMST-wet, QMST-80, and QMST-400, and (b) references of $TiO_2$ (antanse) and montmorillonite.

$$\delta = \rho_W \delta_{W \cdot Xe} + \rho_{Xe} \delta_{Xe \cdot Xe} + \delta_E$$

where $\delta_{W \cdot Xe}$ denotes the influence of collisions between xenon atoms and internal wall of cavity, and $\delta_{Xe \cdot Xe}$ corresponds to the effect of collision between xenon atoms. $\rho_W$ and $\rho_{Xe}$ depend on the density of xenon adsorbed, *i.e.* on the number of xenon atoms per cavity. $\delta_E$ expresses the effect of mean electric field within the cavity. In the present work, since no polarizating cations are present in the cavity of QMST-400, and the sample was dried at 300 °C in a vacuum, and sealed at very low pressure (20 torr) of xenon gas, second and third terms ($\rho_{Xe}\delta_{Xe \cdot Xe}$ and $\delta_E$) could be neglected. If there was no xenon exchange between the pores to a certain degree on NMR time scale, xenon atoms in the pores of different size would show different chemical shifts, and in this case the pore diameter can simply be calculated from the correlation curve between chemical shift and mean free path (t) of xenon[17] as shown in Figure 3(b), although the correlation cannot be complete for pore size calculation by reason of the effect of self-diffusion of xenon, nonuniform pore size, and nonuniform state of surface activation, etc.[18-19] For the case of spherical pores, the pore diameter (D) can be estimated by the following equation;

$$D = 2(t + r_{Xe})$$

where $r_{Xe}$ is van der Waals radius of xenon (2.2 Å).

The $^{129}$Xe NMR spectrum shows two chemical shifts of *ca.* 0 ppm and *ca.* 96 ppm as shown in Figure 3(a). The first chemical shift comes from xenon adsorbed on an external surface, adsorbed in macropore, or nonadsorbed (free), and the second one comes from those adsorbed in micropore of *ca.* 10.4 Å, being analogous to the average slit width calculated from MP method, respectively.

From inconsistency between its micropore size (*ca.* 11.8 Å) and its gallery height (50.4 Å), we can expect that the multistacking (quadruple layer) of nanosized $SiO_2$/$TiO_2$ is present in the interlayer space of montmorillonite (Figure 5).

**Ultraviolet-visible spectroscopy.** UV/Vis spectroscopy gives information on electronic structures such as the

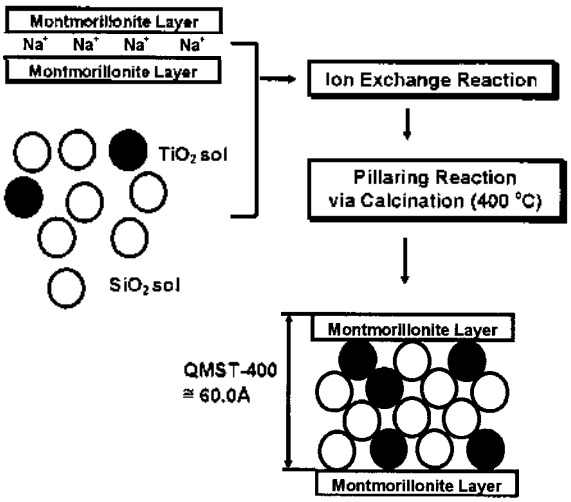


**Figure 5.** Proposed model of the interlayer microstrucutre for QMST-400.

max and the absorption threshold (band gap); the former is the position where the optical absorption attains the maximum and the latter is the position where a steep increase of the optical absorption occurs. And if experimental systems involve quantum sized semiconductors such as $TiO_2$, $ZrO_2$, CdS, ZnS, etc., their size can be deduced from their band gap. Figure 4 shows the UV/Vis spectra of samples together with those of anatase, and Na+ montmorillonite as reference compounds for comparison.

In their optical absorption spectra, there are two important findings to be underlined here; the first one is that QMST-wet exhibits the large blue shift in the absorption threshold and the max compared to the bulk anatase, which is the so-called the quantum confinement,[20-22] due to the presence of $TiO_2$ nanoparticles (*ca.* 20 Å) in the interlayer space of montmorillonite, and the second one is that the red shift in UV/Vis spectra is observed upon calcining QMST-wet at 400 °C owing to a coagulation of $TiO_2$ particles in the interlayer space and/or the formation of Si-O-Ti covalent bonding among intercalated $TiO_2$ sol particles, $SiO_2$ ones, and silicate layers.

## Conclusion

Layered nanocomposite, $SiO_2/TiO_2$ sol pillared clay, has reproducibly been prepared by the ion exchange reaction and its BET surface area is found to be 684 $m^2/g$, which is the highest among various pillared clays ever reported previously. From inconsistency between its micropore size (*ca.* 11.8 Å) and its gallery height (*ca.* 50.4 Å), which calculated using powder XRD, and nitrogen adsorption and $^{129}Xe$ NMR, respectively, we can expect that the quadruple layer of nanosized $SiO_2/TiO_2$ is present in the interlayer space of montmorillonite (Figure 5). And $TiO_2$ particles stabilized in the interlayer space of montmorillonite are found to be quantum-sized of *ca.* 20 Å according to ultraviolet-visible spectroscopy.

**Acknowledgment.** This work was in part supported by the Korea Science and Engineering Foundation through the Center for Molecular Catalysis and by the Ministry of Education (BSRI-97-3413).

## References

1. Pinnavaia, T. J.; Landau, S. D.; Tzou, M. S.; Johnson, I. D. *J. Am. Chem. Soc.* **1985**, *107*, 7222.
2. Jones, S. L. *Catalysis today.* **1987**, *12*, 209.
3. Volzone, C.; Cesio, A. M.; Sanchez, R. M. T.; Peria, E. *Clays & Clay Minerals.* **1993**, *41*, 702.
4. Yamanaka, S.; Doi, T.; Sako, S.; Hattori, M. *Mat. Res. Bull.* **1984**, *19*, 161.
5. Gil, A.; Guiu, G.; Grange, P.; Montes, M. *J. Phys. Chem.* **1994**, *99*, 301.
6. Yamanaka, S.; Nishiharra, T.; Hattori, M. *Mat. Res. Sym.* **1988**, *111*, 283.
7. Yamanaka, S.; Inoue, Y.; Hattori, M.; Okumura, F.; Yoshiikawa, M. *Bull. Chem. Soc. Jpn.* **1992**, *65*, 2494.
8. Takahama, K.; Yokoyama, M.; Hirao, S.; Yamanaka, S.; Hattori, M. *J. Mat. Sci.* **1992**, *27*, 1297.
9. Suib, S. L.; Tanguay, J. F.; Occelli, M. L. *J. Am. Chem. Soc.* **1986**, *108*, 6972.
10. Rudzinski, W. E.; Bard, A. J. *J. Electroanal. Chem.* **1986**, *199*, 323.
11. Giannelis, E. P.; Pinnavaia, T. J.; Rightor, E. G. *J. Am. Chem. Soc.* **1988**, *110*, 3880.
12. Ruhlicke, G.; Niederbudde, E. A. *Clay Minerals* **1985**, *20*, 291.
13. Jameson, C. J.; Jameson, A. K.; Cohen, S. M. *J. Chem. Phys.* **1973**, *59*, 4540.
14. Gregg, S. J.; Sing, K. S. W. *Adsorption, Surface Area and Porosity*, 2nd ed.; Academic Press: London, 1982, pp 94-126.
15. Allen, T. *Particle Size Measurement*, 4th ed.; Chapman and Hall: 1980, pp 540-624.
16. Fraissard, J.; Ito, T. *Zeolites* **1988**, *8*, 350.
17. Demarquay, J.; Fraissard, J. *J. Chem. Phys. Lett.* **1987**, *136*, 314.
18. Karger, J.; Pfeifer, H.; Stallmach, F.; Spindler, H. *Zeolites* **1990**, *10*, 288.
19. Suh, D. J.; Park, T. J.; Ihm, S. K.; Ryoo, R. *J. Phys. Chem.* **1991**, *95*, 3767.
20. Henglen, A. *Chem. Rev.* **1988**, *89*, 1861.
21. Kormann, C.; Bahnemann, D. W.; Michael, R.; Hoffmann, W. M. *J. Phys. Chem.* **1988**, *92*, 5196.
22. Wang, Y.; Herron, N. *J. Phys. Chem.* **1991**, *95*, 525.